AD-A127 660 TIME RESOLVED STUDY OF PRIMARY DECOMPOSITION PROCESS 1/1
FOR NITRO PRAFFINS AND NITRAMINES(U) CORNELL UNIV
ITHACA NY BAKER LAB E R GRANT 15 MAR 83 ARO-16950.9-CH
UNCLASSIFIED DAAG29-80-C-0065 F/G 7/3 NL

END
DATE FILMED
6-83
DTIC

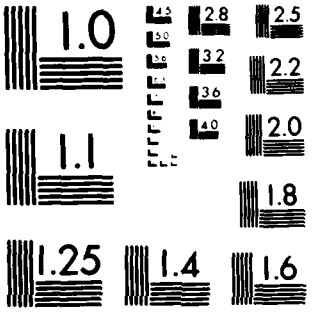

ARO 16950.9-CH

(12)

TIME RESOLVED STUDY OF PRIMARY DECOMPOSITION PROCESSES FOR NITRO PARAFFINS AND NITRAMINES

AD-A127 [illegible]

FINAL REPORT

Edward R. Grant

March 15, 1983

U. S. Army Research Office

DAAG29-80-C-0065

Cornell University

Approved for Public Release
Distribution Unlimited

UNCLASSIFIED
SECURITY CLASSIFICATION OF THIS PAGE (When Data Entered)

REPORT DOCUMENTATION PAGE	READ INSTRUCTIONS BEFORE COMPLETING FORM
1 REPORT NUMBER	2 GOVT ACCESSION NO: AD-A127660 / 3 RECIPIENT'S CATALOG NUMBER
4 TITLE (and Subtitle): Time Resolved Study of Primary Decomposition Processes for Nitro Paraffins and Nitramines	5 TYPE OF REPORT & PERIOD COVERED: Final 1/10/80 - 1/9/83 / 6 PERFORMING ORG. REPORT NUMBER
7 AUTHOR(s): Edward R. Grant	8 CONTRACT OR GRANT NUMBER(s): DAAG29-80-C-0065
9 PERFORMING ORGANIZATION NAME AND ADDRESS: Cornell University, Baker Laboratory, Ithaca, New York 14853	10 PROGRAM ELEMENT, PROJECT, TASK AREA & WORK UNIT NUMBERS
11 CONTROLLING OFFICE NAME AND ADDRESS: U. S. Army Research Office, Post Office Box 12211, Research Triangle Park, NC 27709	12 REPORT DATE: March 15, 1983 / 13 NUMBER OF PAGES: 25
14 MONITORING AGENCY NAME & ADDRESS(if different from Controlling Office)	15 SECURITY CLASS. (of this report): Unclassified / 15a DECLASSIFICATION DOWNGRADING SCHEDULE

16 DISTRIBUTION STATEMENT (of this Report):

Approved for public release; distribution unlimited.

17 DISTRIBUTION STATEMENT (of the abstract entered in Block 20, if different from Report)

NA

18 SUPPLEMENTARY NOTES

The view, opinions, and/or findings contained in this report are those of the author(s) and should not be construed as an official Department of the Army position, policy, or decision, unless so designated by other documentation.

19 KEY WORDS (Continue on reverse side if necessary and identify by block number)

Energetic Materials
Unimolecular Decomposition
Primary Reactions
Nitro Paraffins
Nitramines
Molecular Beams
Infrared Multiphoton Dissociation
Multiphoton Ionization

20 ABSTRACT (Continue on reverse side if necessary and identify by block number)

A molecular beam unimolecular fragmentation mass spectrometer has been developed and applied to the study of primary dissociation processes in energetic materials. The experimental approach uses infrared multiphoton excitation to prepare isolated molecules in the beam for dissociation. Visible laser induced multiphoton

DD FORM 1 JAN 73 1473 EDITION OF 1 NOV 65 IS OBSOLETE

UNCLASSIFIED
SECURITY CLASSIFICATION OF THIS PAGE (When Data Entered)

ionization detects products with time-of-flight, scattering angle and internal quantum state resolution. This report describes the method, spectroscopic results on CH_3^{Γ} and NO_2^{Γ}, experimental observations on the primary decomposition dynamics of $CH_3^{\Gamma}NO_2^{\Gamma}$, and their theoretical interpretation.

I. Introduction

The principal objective of the work reported here has been to study the problem of dynamical characterization of the primary decomposition processes of energetic materials, nitro paraffins and nitramines. It has been our aim to develop a general method for the initiation and detailed observation of the consequences of unimolecular fragmentation of such materials under collision-free, molecular beam conditions. The initial phases of our work have been concerned with the construction of the instrument and the execution of necessary developmental experiments establishing the applicability of our detection method, time-resolved multiphoton ionization, to compounds expected as fragmentation products. Our work in this contract period has culminated in the experiment bringing all of these preliminary elements together in a fully resolved experiment characterizing the dynamics of C-N bond scission in the decomposition of nitromethane.

This report gives a summary account of the accomplishments of our work under contract DAAG29-80-C-0065. Listed in order of presentation in the following sections, these accomplishments include: 1) Devlopment of a laser ionization mass spectrometric apparatus for the study of multiphoton spectroscopy and unimolecular fragmentation dynamics; 2) Complete elucidation of the role of photodissociation dynamics in the multiphoton ionization of NO_2 from 400 to 500 nm; 3) Assignment of the 500 to 520 nm four photon Rydberg system that yields resonance enhanced production of NO_2^+ with internal state distribution information;

4) Detection of CH_3 and NO_2 products from the collision-free decomposition of CH_3NO_2 with spectroscopic internal state, and angular and time-of-flight velocity resolution; 5) Development of a direct count, detailed angular momentum conserving excluded phase space model for energy disposal in unimolecular decomposition as a statistical framework for the analysis of experimental energy disposition results; and 6) Broadening of the application of multiphoton ionization to include demonstration of its utility as a combustion diagnostic.

II. Progress Report

A. Laser Ionization Mass Spectrometric Apparatus for Studies of Spectroscopy and Reaction Dynamics

We have developed an instrument for mass resolved studies of multiphoton ionization as a probe in the study of unimolecular reaction dynamics.[1-11]* It consists of an extranuclear quadrupole mass spectrometer contained within a stainless steel vacuum chamber fitted with a pulsed molecular beam source and optics for admitting UV/visible and infrared laser light.

Figure 1 shows a schematic of the apparatus as configured for a MPD/MPI experiment. To start such an experiment a 10 Hz trigger signal of a single clock circuit is split into two parallel lines. The master clock signal triggers a Quanta-Ray DCR-1A/PDL-1 YAG-pumped tunable dye laser, which has a 3 ms internal command rise time. Delayed appropriately with respect

---

* References keyed to list of ARO supported publications.

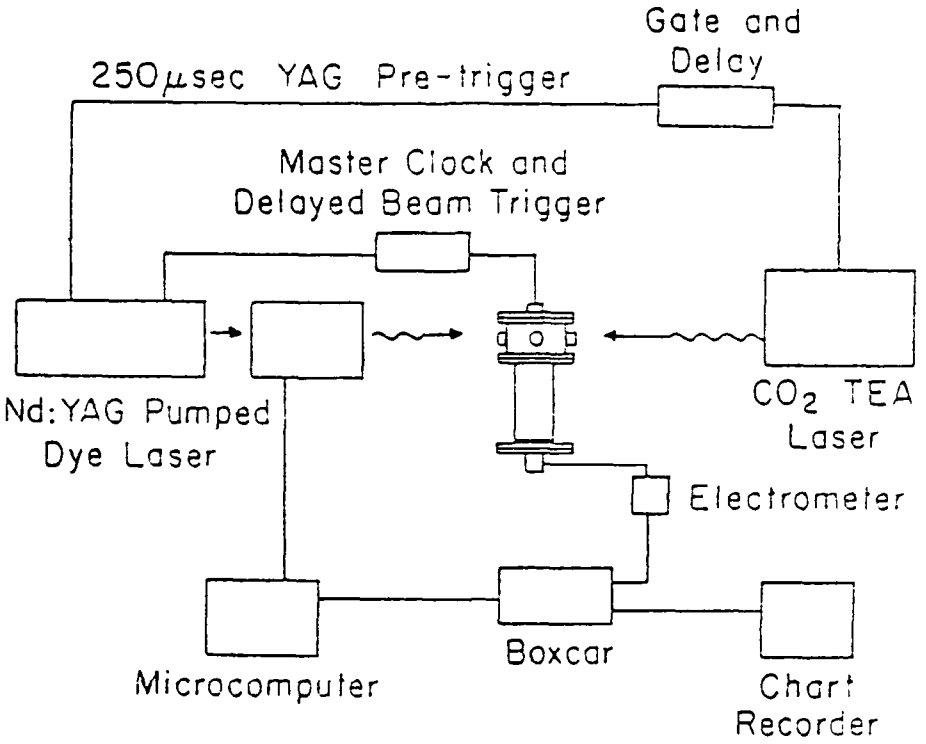

Figure 1. Schematic view of the MPD/MPI dissociation and detection apparatus, including the triggering and signal processing electronics. The vacuum chamber contains the ion optics, quadrupole mass spectrometer, and particle multiplier.

to this start pulse, a second line triggers an electromagnetic valve, admitting a pulsed supersonic beam of the sample gas down the axis of the vacuum chamber. The valve produces a 70 μs rotationally cooled pulse. A six inch Varian diffusion pump, combined with an Air Products Displex refrigerated cold trap, clears the chamber to a pressure of 2×10^{-7} Torr between pulses. The YAG laser provides a 250 μs pre-trigger pulse, which starts a high-resolution adjustable gate and delay. The output of this device, after eight-fold division in frequency, triggers a home-built grating tuned CO_2 TEA laser. The 1.25 Hz repetition rate of this laser limits the present rate of data collection. This timing arrangement ensures that the CO_2 laser fires through

the peak of the molecular beam intensity and that the dye laser fires at a precisely specified time shortly thereafter.

The pulse of light from the CO_2 laser passes through an eight inch focal length Ge lens, enters the vacuum system horizontally through a NaCl window, and focuses in the path of the molecular beam. The high intensity of the light induces MPD in a fraction of the sample molecules within the focal volume. The pulse of visible light from the dye laser passes through an eight inch focal length quartz lens, enters the vacuum system from above, and focuses at the intersection of the CO_2 laser and molecular beams. When tuned to a single- or multi-photon resonant absorption of one of the dissociation fragments, this pulse selectively ionizes the molecules of that fragment in a multiphoton process.

An ion optics assembly (API-272-N2), manufactured by Extranuclear Laboratories, surrounds the interaction region of the three beams and collects and focuses the resulting ions into the entrance of an Extranuclear quadrupole mass spectrometer (ELFS 4-324-9). Those ions passing through the quadrupole receive a 10^7 gain in a particle multiplier (Gallileo Electro Optics Channeltron 4816). The detection process thus embodies both wavelength and mass discrimination against ions produced from the parent molecule or from other dissociation fragments.

A Keithley 427 electrometer converts current to voltage and amplifies the signal for averaging by a PAR 164/162 boxcar that samples at the repetition rate of the CO_2 laser. As discussed later, to acquire data on internal states of products we hold the

position and delay times of the probe laser constant while we scan the wavelength of the dye laser. To determine fragment recoil velocities, we hold wavelength constant and scan angular position and delay time. In all cases a chart recorder displays the output of the boxcar signal averager.

But for the absence of the CO_2 laser and its attendant timing electronics, the apparatus and procedure are the same for pure MPI spectroscopic experiments.

B. Photodissociation Dynamics and Multiphoton Ionization Spectroscopy

MPI characterization of a compound is an essential step toward its detection as a reaction fragment. This is especially true where complex, dissociative paths to photoionization are possible, and thus is a strong motivating factor in our studies of the multiphoton ionization spectroscopy of NO_2.[3,6,7,9]

Figure 2 shows an energy diagram illustrating the electronic states and photodissociation pathways involved in the multiphoton ionization of NO_2. We find from our experiments that for wavelengths shorter than 500 nm, dissociation at the level of the second photon dominates the laser driven process; in our laser/mass spectrometric apparatus we see only NO^+ from the ionization of the nascent, neutral NO photoproduct. At wavelengths longer than 500 nm we are able to detect NO_2^+. The spectrum in this latter region is characteristic of the initial NO_2 distribution and thus useful as a probe of the dynamics of NO_2 producing reactions. The assignment of the resonance system leading to NO_2^+ is given in the next section.

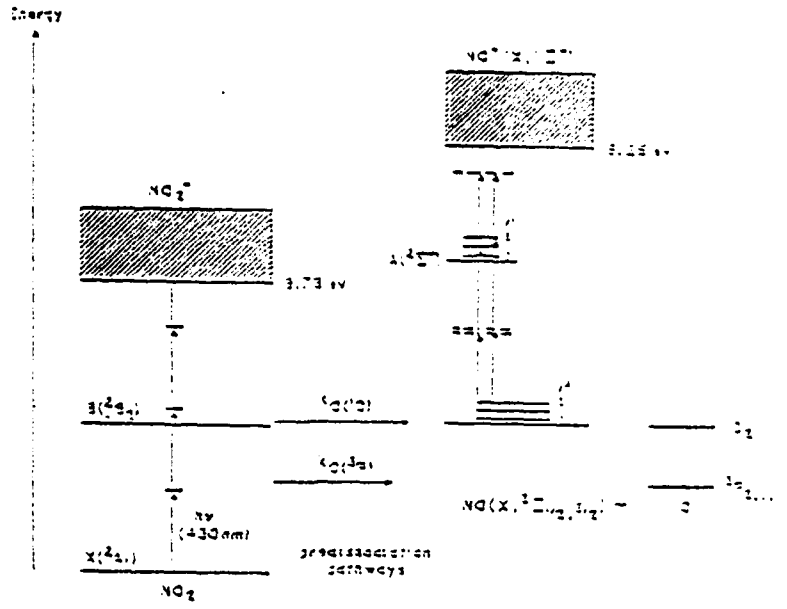

Figure 1. Multiphoton ionization scheme for the detection of nascent O produced in the two-photon dissociation of NO_2.

Behavior in the region of two photon dissociation is most interesting, bringing to light states and nonradiative pathways that appear to be accessible only by non-linear excitation. Briefly, in two photon excitation to just above the origin of $\tilde{B}^2B_2$, below the thermochemical threshold for production of $O(^1D)$, we observe an ionization spectrum characteristic of rotationally and vibrationally hot NO, consistent with the large amount of excess energy available 15,000 cm^{-1} above the threshold for formation of ground state $NO(\tilde{X}^2\pi)$ and $O(^3P)$.

As we tune to the blue so that our two photon energy crosses the threshold for production of $O(^1D)$ we see a dramatic change in the NO_2 MPI spectrum. As Figure 3 shows, but for the presence of sequence bands and somewhat broader rotational envelopes, it now closely resembles the spectrum of room temperature NO. Clearly,

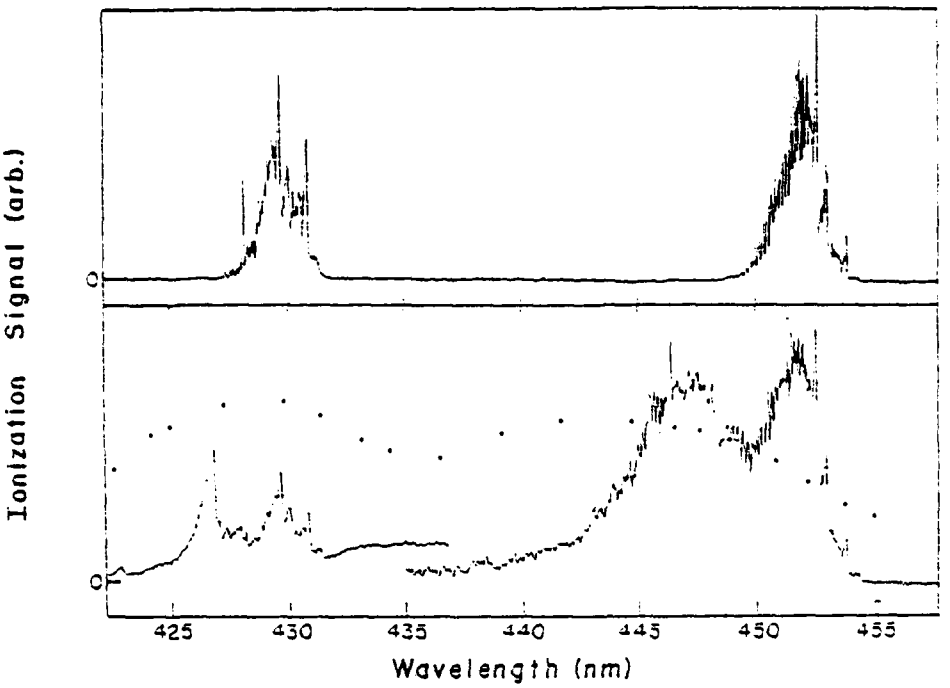

Figure 3.

NO⁺ MPI spectrum of NO_2 between 455 and 420 nm (lower frame) compared with the corresponding spectrum of NO (upper frame). Dots indicate dye laser intensity.

soon after it is accessible, the $O(^1D)$ channel dominates leaving much less energy available to deposit in the internal degrees of freedom of the product NO.

We have examined this 420 to 450 nm region of the NO_2 MPI spectrum in detail, using supersonically cooled NO_2 expanded from a pulsed jet. In general our high resolution experiments confirm the observations made above for static cell samples; for the most part the internal energy distribution in the nascent NO resulting from photodissociation of NO_2 at the two photon level via the $O(^1D)$ pathway qualitatively resembles that observed in the near UV, one photon dissociation of NO_2 via the $O(^3P)$ pathway for which there is a similar excess energy above threshold. As shown in Figure 4, for two photon photolysis near 450 nm, we observe the production of both NO spin-orbit components. Vibrational and

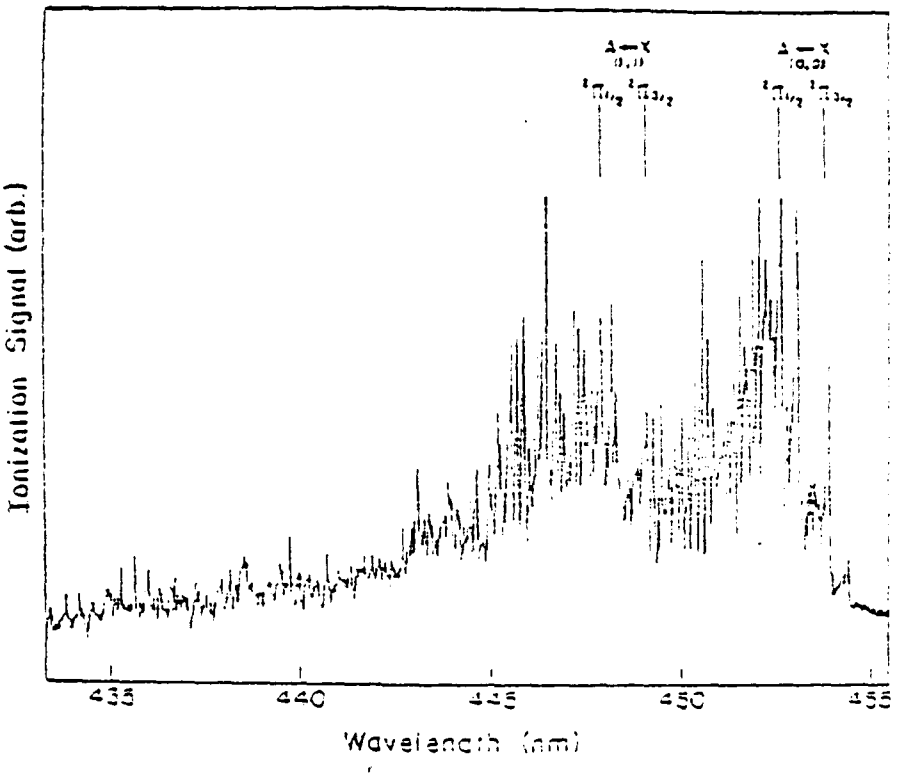

Figure 4. Molecular beam MPI spectrum of NO^+ from NO_2 in the 430 nm sequence region.

rotational excitation in the nascent NO are consistent with dissociation from the bent $\tilde{B}^2B_2$ upper state of NO_2.

However, in the neighborhood of 427 nm, the NO internal state distribution is dramatically different. For NO in v"=1, observed by means of the resonance $\tilde{A}^2\Sigma^+(v'=2) \leftarrow \tilde{X}^2\pi(v"=1)$, presented in Figure 5, we find that the photoproduct rotational distribution is extraordinarily cold, limited by the rotational temperature of our supersonic molecular beam, and that a spin-orbit component $^2\pi_{1/2}$, is missing. Our data thus indicates that the dissociation dynamics are radically different in this spectral region, suggesting a linear or near-linear dissociation geometry that imparts very little torque to the departing NO photo-

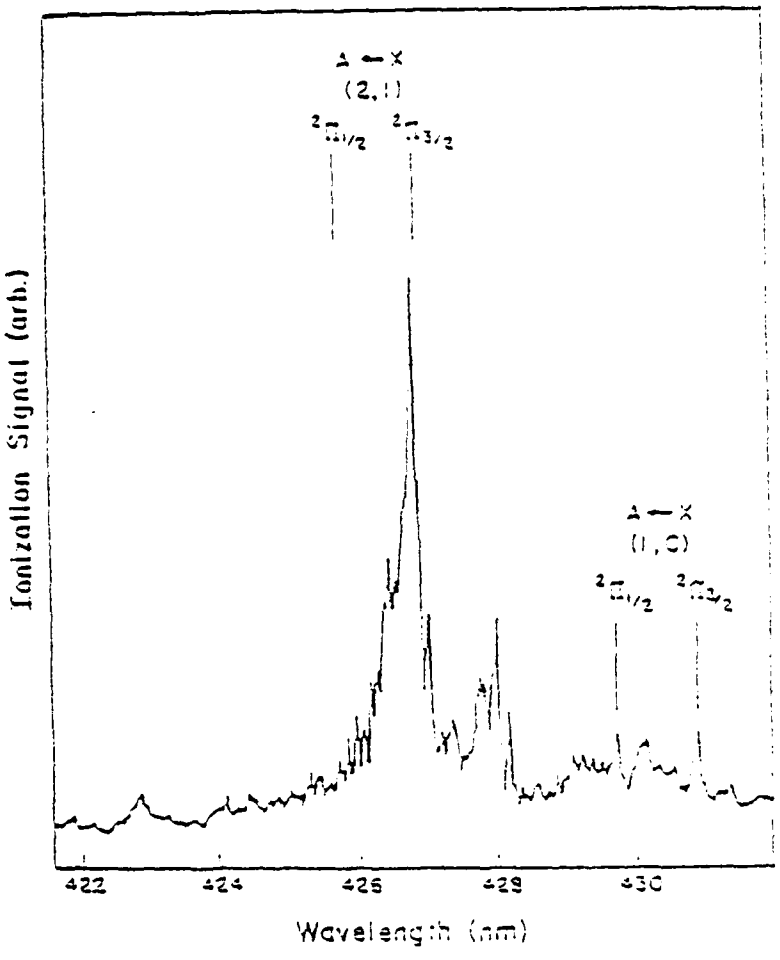

Figure 3. Molecular beam MPI spectrum of NO^- from NO_2 in the 430 nm sequence region.

fragment, and places strict symmetry requirements on its spin-orbit state. We assign the source of this behavior to the participation of the theoretically calculated but never observed $(...1\pi_g^4 5\sigma_g)\ ^2\Sigma_g^+$ linear excited state of NO_2 lying above the origin of $\tilde{B}^2B_2$.

C. Assignment of the Resonant Features Associated with:

$NO_2 \xrightarrow{5h\nu} NO_2^+$

As indicated above for wavelengths longer than 500 nm, where the energy of two photons falls short of the origin of $\tilde{B}^2B_2$, continued pumping apparently competes effectively with dissociation because we observe the production of NO_2^+. The spectrum of this ionization signal is characterized by resonances at the level of the fourth photon with high lying members of the NO_2 npσ (0,1,0) Rydberg series. The elements of this series as they appear in the MPI spectrum of NO_2 are shown with their assignment in Figure 6. This assignment fits precisely on the low energy side with the 3pσ Rydberg state observed in one photon absorption. Accounting for the vibrational state of the core, we converge on the high energy side to an adiabatic ionization potential of 9.78 eV.

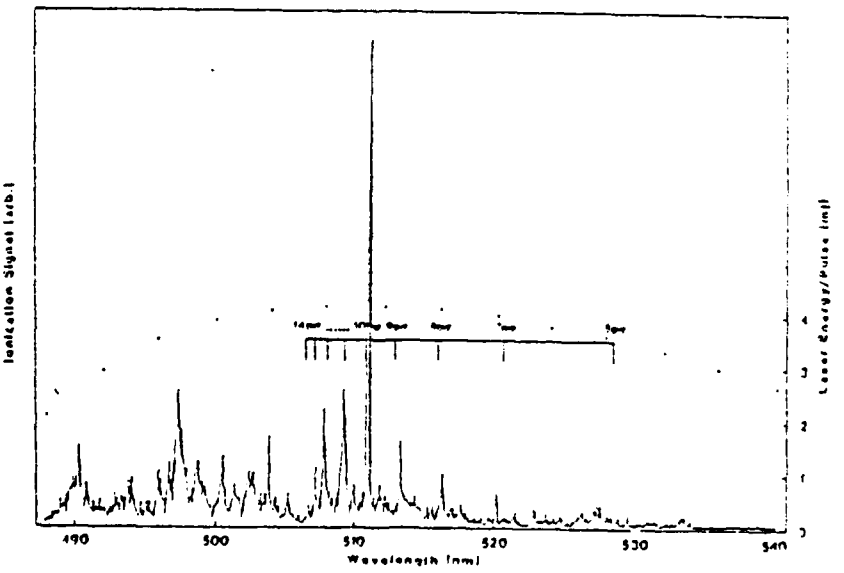

Figure 6. Multiphoton ionization spectrum of NO_2 in a supersonic jet showing elements of the npσ Rydberg state resonance system.

Our assignment of the vibrational quantum number of the upper state in this progression is confirmed by an analysis of a high resolution, pressure-tuned etalon scan of the single prominent member at 511 nm. The experimental spectrum is shown in Figure 7. Figure 8 gives a computer simulation of the spectrum of this transition assigned as a four-photon

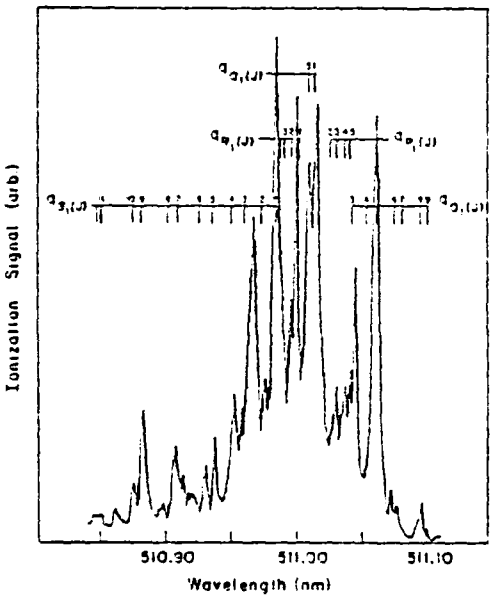

Figure 7. High resolution pressure tuned etalon scan of the 511 nm resonant feature.

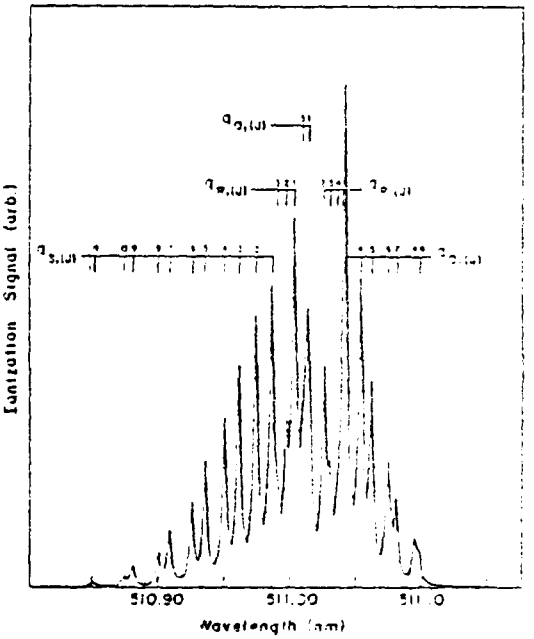

Figure 8. High resolution computer simulation of the NO_2 four photon parallel transition. $\tilde{C}^2B_2$ (10,2a) (0,1,0) $\leftarrow$ $\tilde{X}^2A_1$ (0,0,0) K = 1.

bent-to-linear parallel transition from $\tilde{X}^2A_1$ (0,0,0) K=1 to $\tilde{E}^2\Sigma_u^+$ (10 pσ) (0,1,0) ℓ = 1, where K is the projection of the rotational angular momentum on the symmetric top axis and ℓ is the vibrational angular momentum of the linear excited state. The full range of J is allowed. The requirement for vibrational angular momentum fixes the bending quantum number of the linear upper state. Four photon line-stength factors are included in the simulation.

D. Dynamics of the Decomposition of Nitromethane: Detection of CH_3 and NO_2 Products with Internal State and Velocity Resolution

Multiphoton ionization spectra of CH_3 and NO_2 products from infrared laser induced unimolecular decomposition of CH_3NO_2 are shown in Figures 9 and 10. These spectra were obtained with superimposed pump and probe laser beams, and thus represent an average over all products. Comparison with thermal data, our own for NO_2 and that of others for CH_3 (see ref. 10), suggest that our distributions, while not necessarily Boltzmann, have average energies the order of room temperature.

The angular distribution of products scattered out of the beam by recoil associated with unimolecular decomposition is determined by scanning the focus of the probe through an arc radially displaced 5mm from the scattering center. The results of such a scan for CH^3 and NO^2 are given in Figure 11.

Close inspection of these data reveal that taken together the two distributions appear to violate linear momentum conservation; the lighter CH_3 fragment should be scattered to larger

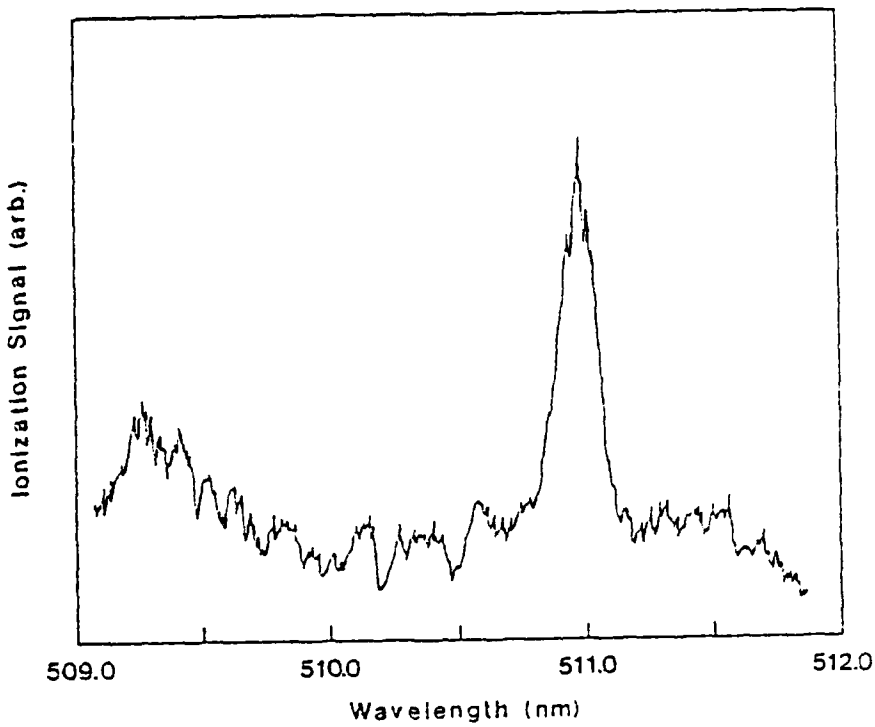

Figure 9. Multiphoton ionization spectrum of the NO_2 fragment produced by infrared multiphoton dissociation of CH_3NO_2.

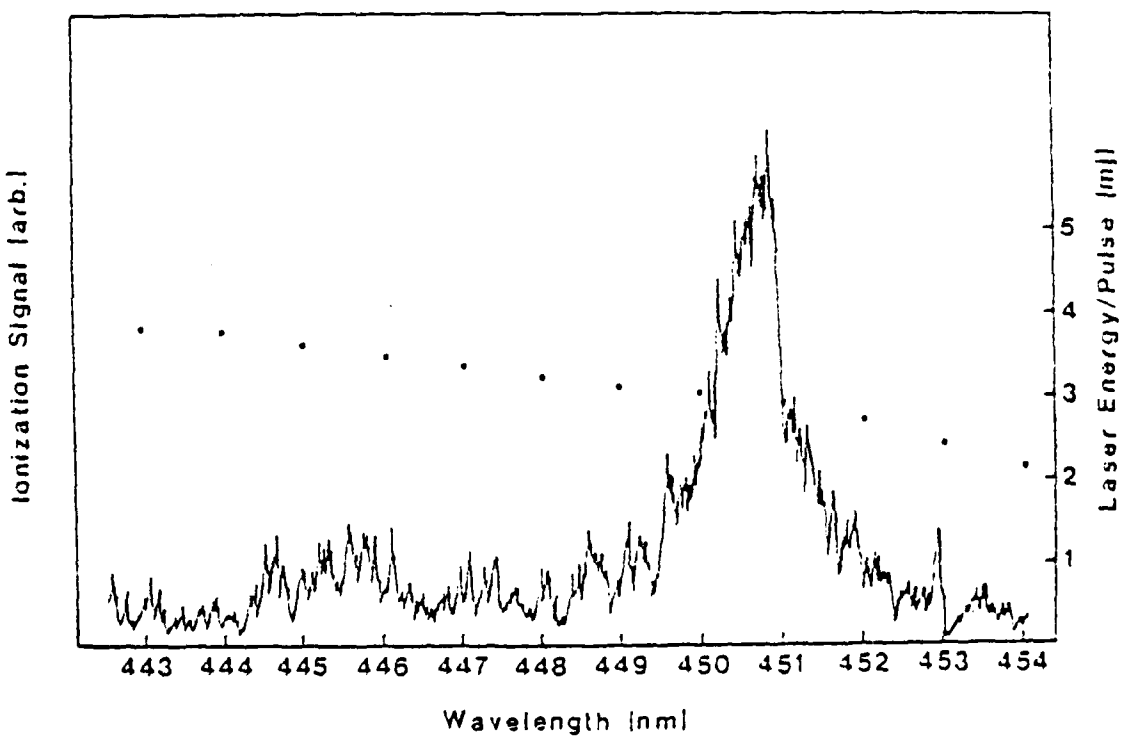

Figure 10. Multiphoton ionization spectrum of the CH_3 fragment produced by infrared multiphoton dissociation of CH_3NO_2.

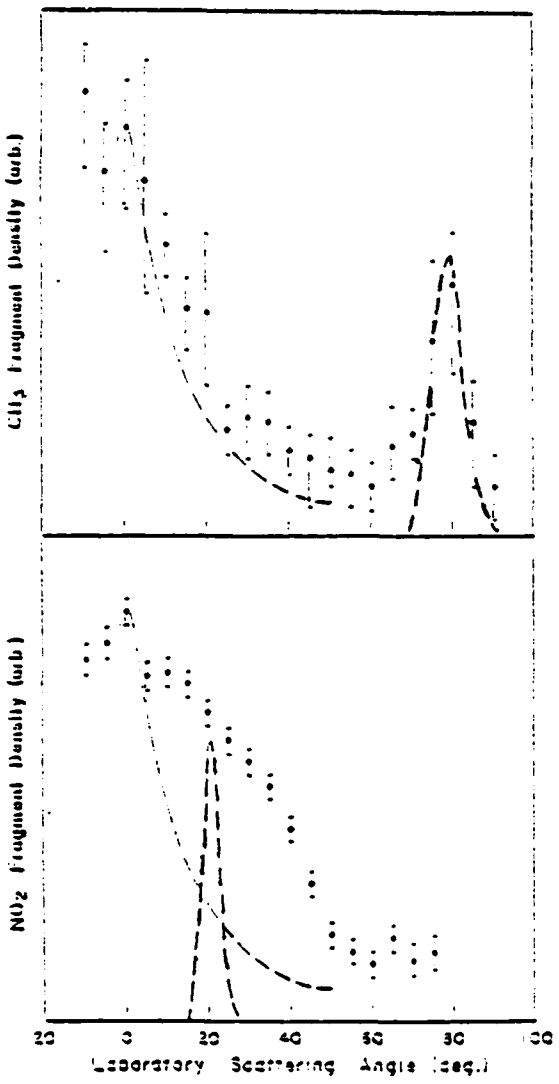

Figure 11. Angular distribution of the CH_3 (top) and NO_2 (bottom) resulting from the multiphoton dissociation of CH_3NO_2. Both distributions reflect the signal strength with a flight path of 5mm and a delay of 4 μsec between the dissociating and ionizing laser pulses. (— — —) apparent angular distribution produced by ionization of the parent beam, determined by separate measurement. (— — —). Theoretical CH_3 and NO_2 laboratory angular distributions obtained by computer simulation for a center-of-mass recoil energy sharply peaked at 1500 cm^{-1}.

laboratory angles. In contrast, Figure 11 shows the CH_3 signal falling off at 30° while the NO_2 signal falls off at 50°.

We believe that each figure actually contains the signal contributions of two photoproducts. The narrow distribution is caused by dissociative ionization of laser heated CH_3NO_2 contained within the parent beam. (Its 1mm half-width coupled with our short, 5mm probe radius gives this component its apparent

angular distribution.) A separate determination of this distribution for our present beam source-skimmer geometry is indicated by the fine dashed lines in Figure 11. The bold dashed lines show calculated laboratory distributions for CH_3 and NO_2 given a center-of-mass recoil energy release peaked sharply at 2500 cm^{-1}.

E. Theoretical Analysis of Energy Disposal in Unimolecular Decomposition to Polyatomic Fragments

Our MPD/MPI molecular beam scattering experiments have given us information about the internal state populations as well as the recoil velocities of both CH_3 and NO_2 fragments of the decomposition of nitromethane. The question immediately emerges are all of these distributions consistent with each other? (Do the rotational distributions match when one considers angular momentum conservation? Is the energy content of the rotational degrees of freedom consistent with that found in translation?) Also, do all these energy distributions sensibly match with what one might expect to see statistically, or are dynamical factors at work determining the distribution of excess energy?

To analyze our data in a way that addresses these questions we have developed a direct count phase space theory algorithm to precisely predict the statistical expectations for translations rotations and vibrations, explicitly conserving angular momentum and energy.[10] This algorithm takes advantage of two factors that make a detailed direct count over vibrational and rotational states possible:

1) With reactant expanded in a molecular beam, and, presumably,

not rotationally excited to a significant degree by the infrared laser, the total angular momentum to be conserved by our calculation is a simple quantity, to a first approximation, zero.

2) To perform the computation, we use a fast state counting algorithm developed originally to direct count vibrational states. With this algorithm the full computation, for a moderate level of available energy, uses only a few minutes of computer time.

Briefly the following steps are employed to determine the statistical distribution of a given amount of energy in excess of the decomposition threshold: A direct count over vibrational states produces a map of accessible vibrational energy levels and degeneracies. A rotational count is then performed for each vibrational level, and the results combined to form a total probability distribution.

To carry out each rotational count we individually index total angular momentum quantum numbers, J_{CH_3} and J_{NO_2} for each fragment. For each combination we consider all space quantized projections, choosing for each an interfragment orbital angular momentum that conserves the total zero angular momentum of the system. The energies and degeneracies of each molecule fixed projection are then considered, and all combinations that conserve energy are weighted properly and added to appropriate running distributions.

For an average excess energy of 1000 cm^{-1}, we obtain the distributions of CH_3 and NO_2 rotational quantum numbers and

relative translational energy given in Figures 12 and 13, respectively.

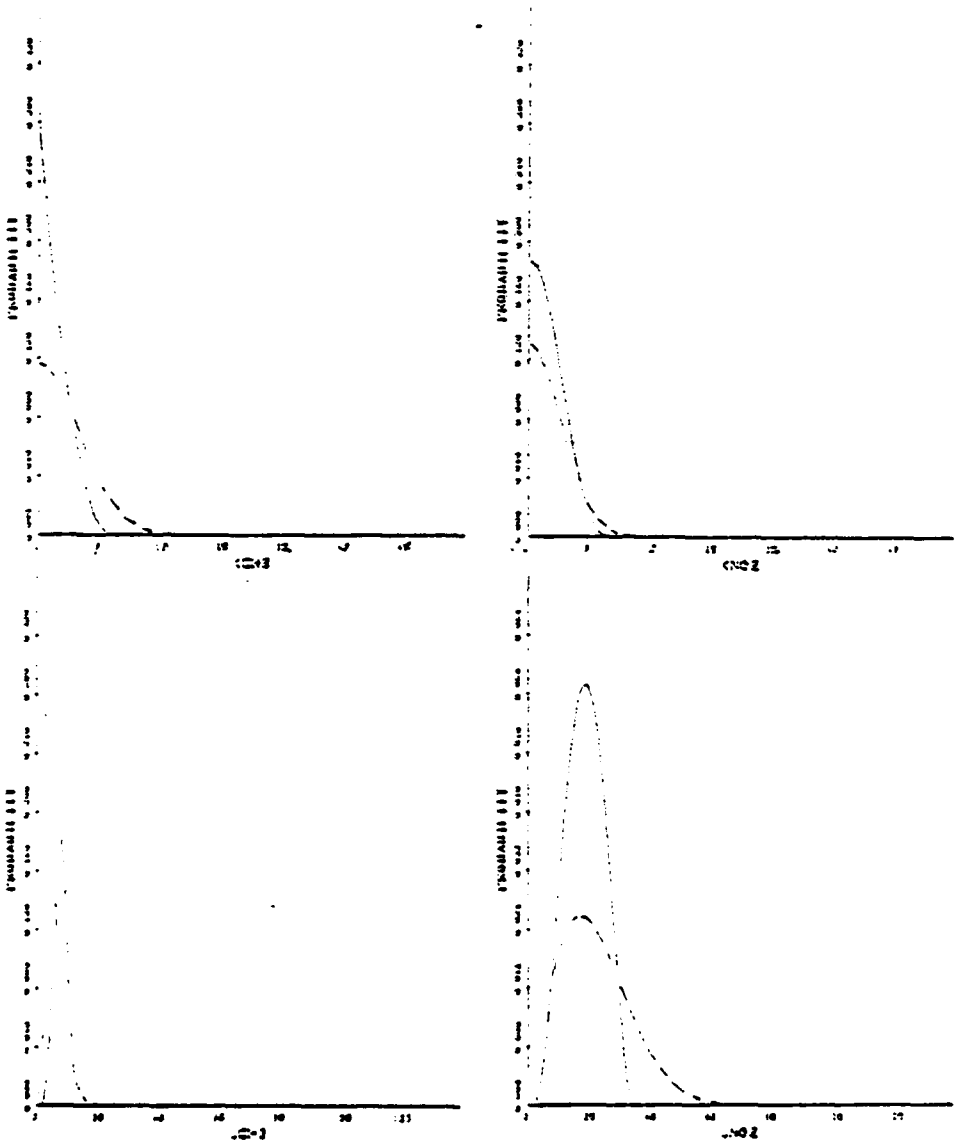

Figure 12. Direct count excluded phase space theory rotational quantum number distributions for NO_2 and CH_3 reflecting the statistical partitioning of 1000 cm^{-1} excess energy. Dashed lines show the corresponding 400°K Boltzmann distribution for comparison.

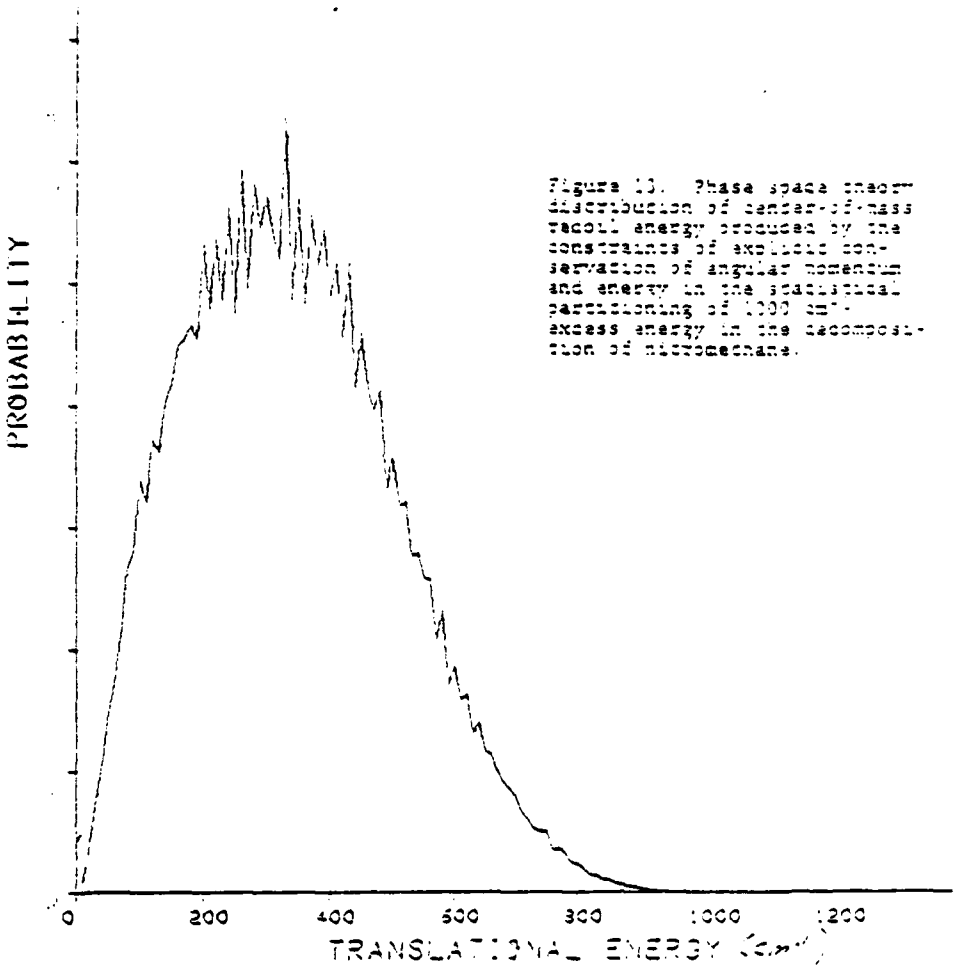

Figure 13. Phase space theory distribution of center-of-mass recoil energy produced by the constraints of explicit conservation of angular momentum and energy in the statistical partitioning of 1000 cm⁻¹ excess energy in the decomposition of nitromethane.

It is important to note that while rigorously statistical, none of these distributions are thermal. For reference 400°K thermal distributions are dashed in on each of the rotational quantum number plots.

This difference has important consequences. We compare theoretical to experimental results by taking tabular distributions over rotational quantum numbers output by our phase space program as input to a program that produces spectral simulations of NO_2 and CH_3 multiphoton resonances. Results of this procedure for

1000 cm^{-1} excess energy are shown together with experimental scans in Figures 14 and 15. While the agreement here is very good, it is most important to note that no thermal distribution will fit either spectrum. Thus we appear to have in the experimentally observed rotational populations, a direct confirmation of our phase space model for energy disposal in unimolecular decomposition to polyatomic fragments.

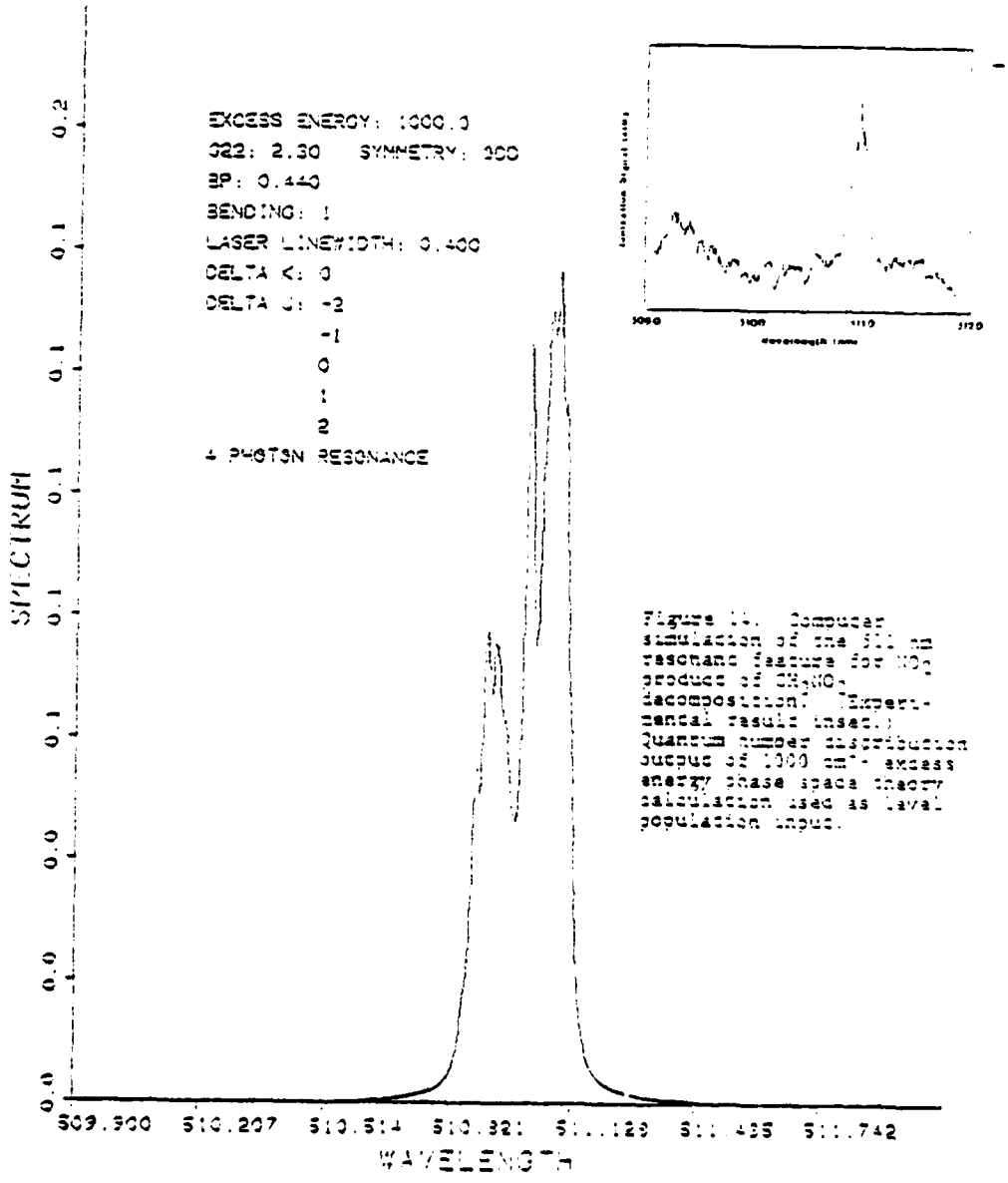

Figure 14. Computer simulation of the 511 nm resonant feature for NO_2 product of CH_3NO_2 decomposition. (Experimental result inset.) Quantum number distribution output of 1000 cm^{-1} excess energy phase space theory calculation used as input population input.

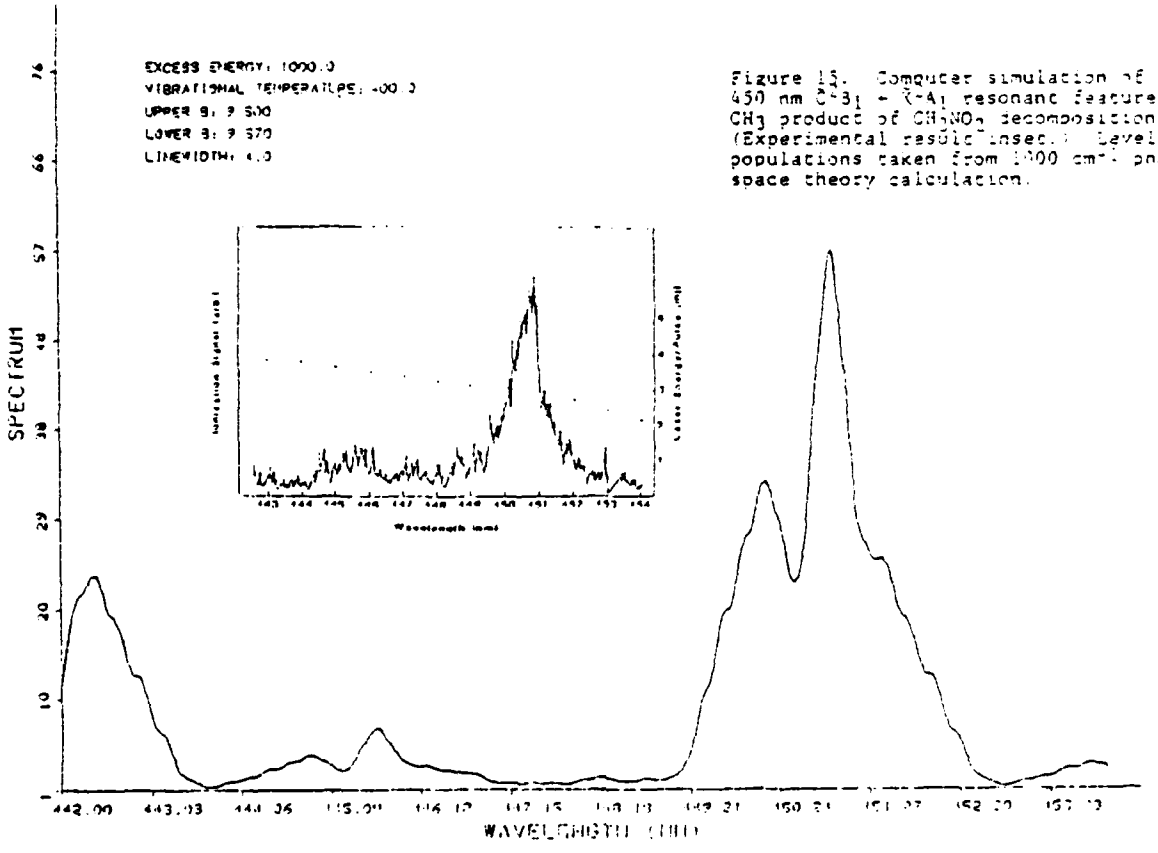

Figure 15. Computer simulation of the 450 nm $\tilde{C}^1B_1 - \tilde{X}^1A_1$ resonant feature for CH_3 product of CH_3NO_2 decomposition. (Experimental results inset.) Level populations taken from 1000 cm^{-1} phase space theory calculation.

It is now instructive to inquire about the agreement between predicted and observed translational energy distribution. Recall the experimental results suggest a distribution peaked about an average the order of 2500 cm^{-1}. The translational energy distribution shown in Figure 13 is not nearly that energetic. So we must conclude that our model, validated for rotational energy disposal, significantly underestimates the translational energy of recoiling CH_3 and NO_2 fragments. Dynamical factors must be at work: There must be an added source of energy deposited into recoil as fragments separate. We suspect relaxation associated

with the geometry changes of CH_3 and NO_2, act to produce a barrier in the exit channel. Should this surface feature be confirmed, it will have a profound effect on the theoretical framework for decomposition kinetics in this simplest of nitroparaffins.

F. Multiphoton Inization as a Combustin Diagnostic

We have demonstrated the utility of multiphoton ionization as a combustion diagnostic by obtaining the spectrum and concentration profile of nascent NO in a premixed laminar methane/air flame.[4]

Figure 16 shows the spectrum of the transient ion current produced by the dye laser focussed between collection wires in the flame. We assign this spectrum to NO. Figure 17 demonstrates the spatial resolution of the tightly focussed laser beam. As the burner is lowered from near contact with the laser

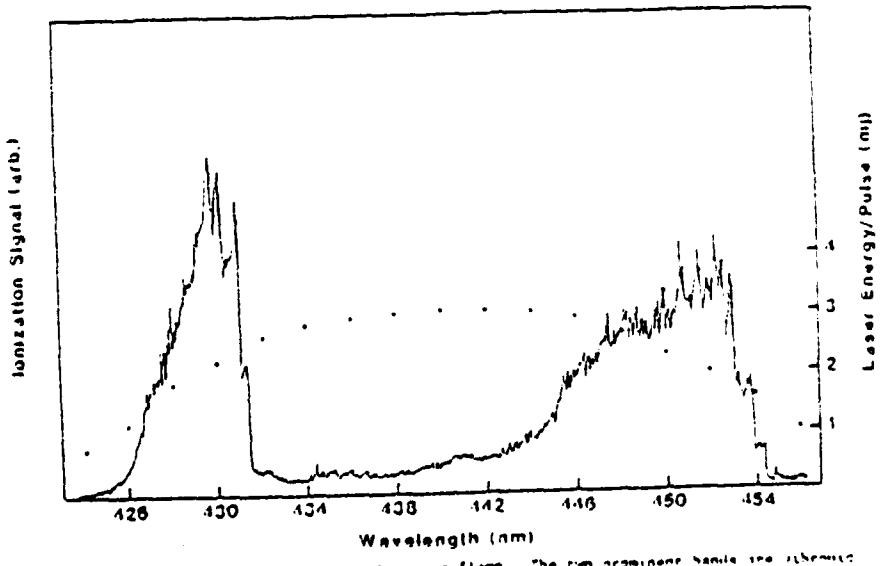

Figure 16. MPI spectrum of NO in a methane/air flame. The [illegible] bands are [illegible] members of the well-known two-photon transition [illegible]

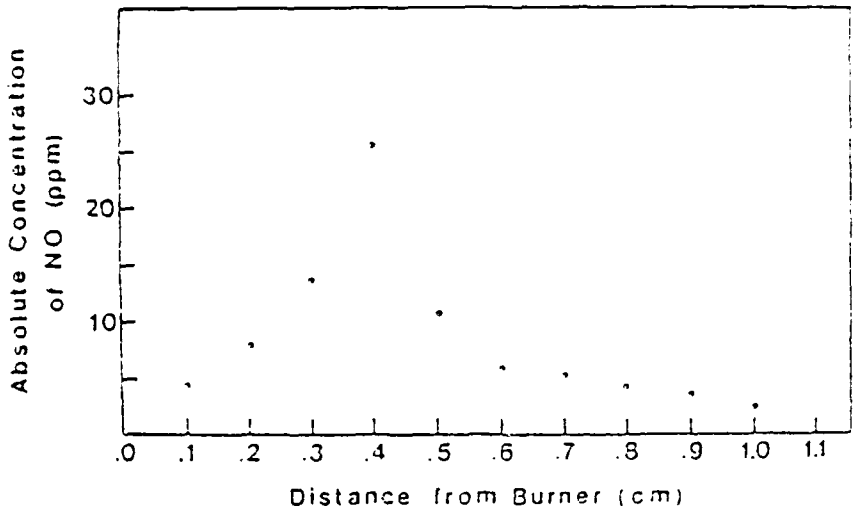

Figure 12. Absolute concentration of NO in the flame as a function of distance from the burner. The transition from the luminous to dim portion of the flame occurs 1mm from the burner.

focus, changing the position of the focus in the flame, the ionization signal at 450 nm first increases sharply and then decreases. The region of maximum signal is about a millimeter beyond the sharp transition from bright to dim blue flame.

List of Publications of Work Supported by ARO

1. Resonant Multiphoton Ionization Detection of the NO_2 Fragment from Infrared Multiphoton Dissociation of CH_3NO_2, B.H. Rockney and E.R. Grant, Chem. Phys. Lett. 79, 15 (1981).

2. Two-Photon Resonant Multiphoton Ionization Spectroscopy: A New Rydberg System in Br_2, R.J.S. Morrison and E. R. Grant, J. Chem. Phys. 75, 49 (1981).

3. Multiphoton Ionization of NO_2: Spectroscopy and Dynamics, R.J.S. Morrison, B.H. Rockney and E.R. Grant, J. Chem. Phys. 75, 2643 (1981).

4. Detection of Nascent NO in a Methane/Air Flame by Multiphoton Ionization, B.H. Rockney, T.A. Cool and E.R. Grant, Chem Phys. Lett. 87, 141 (1982).

5. $\tilde{A}^1\pi \leftarrow \tilde{X}^1\Sigma^+$ Resonance-Enhanced Multiphoton Ionization of Jet-Cooled CO, R.W. Jones, N. Sivakumar, B.H. Rockney, P.L. Houston and E.R. Grant, Chem. Phys. Lett. 91, 271 (1982).

6. Two-Photon Photodissociation Dynamics of NO_2 in the Region of 45,000 cm^{-1}, R.J.S. Morrison and E.R. Grant, Proceedings of the 15th Informal Conference on Photochemistry, Stanford, CA, June, 1982.

7. Dynamics of the Two Photon Photodissociation of NO_2: A Molecular Beam Multiphoton Ionization Study of NO Photofragment Internal Energy Distributions, R.J.S. Morrison and E.R. Grant, J. Chem. Phys. 77, 5994 (1982).

8. Detection of Photofragments by Multiphoton Ionization with Direct Resolution of Angular and Time-of-Flight Distributions, B.H. Rockney and E.R. Grant, J. Chem. Phys. 77, 4257 (1982).

9. Resonance Multiphoton Ionization of Nitrogen Dioxide: Four-Photon Spectroscopy of the npσ Rydberg Series, B.H. Rockney, G.E. Hall and E.R. Grant, J. Chem. Phys. 78, xxxx (1983).

10. Unimolecular Decomposition of Nitromethane in a Molecular Beam with Resolution of Fragment Recoil Velocities and Internal States: Dynamical Evidence for an Exit Channel Barrier, B.H. Rockney and E.R. Grant, J. Chem. Phys. 79, xxx (1983).

11. Highly-Efficient Production of Neutral Carbon Atom in the Ultraviolet Multiphoton Fragmentation of Aromatic Molecules, R.L. Whetten, K.J. Fu, R.S. Tapper and E.R. Grant, J. Phys. Chem. 87, xxx (1983).

Participating Scientific Personnel

Past Personnel with Defrees Conferred

Richard J. S. Morrison	Ph.D.	1982
Bennet H. Rockney	Ph.D.	1982
Alizd I. Wechsler	M.S.	1981
Paul W. Fairchild	Postdoctoral Research Associate	

Present Personnel

Laurence Bigio

Dr. Fu Ke-Jian (Visiting Scientist)

Rochelle Tapper

Douglas A. Webb

Robert L. Whetten (NSF Fellow)


DATE
FILME